Hindawi
Advances in Civil Engineering
Volume 2019, Article ID 3129485, 11 pages
https://doi.org/10.1155/2019/3129485

Research Article

Asphalt Pavement Mechanical Response of Accelerated Pavement Testing in Single-Axle and Dual-Axle Loading Modes

Zhiguang Guan,[1] **Chuanyi Zhuang**,[2] **and Peng Zhang**[1]

[1]*School of Mechanical Engineering, Shandong Jiaotong University, Jinan, Shandong 250023, China*
[2]*School of Civil Engineering, Shandong Jiaotong University, Jinan, Shandong 250023, China*

Correspondence should be addressed to Zhiguang Guan; guanzhiguang@sdjtu.edu.cn

Received 20 November 2018; Revised 30 January 2019; Accepted 28 February 2019; Published 1 April 2019

Academic Editor: Xu Yang

The objective of this study is to evaluate the influence of moving loads on the asphalt pavement in response to single-axle and dual-axle loading modes using the full-scale accelerated pavement testing (APT) facility from Shandong Jiaotong University. First, a test lane of pavement with four structures is constructed. Eleven strain sensors and four pressure cells are embedded at different depths and positions. Secondly, a research on the strain and stress in single-axle and dual-axle loading modes is conducted. Finally, the time accumulation of strain and stress is defined to describe the degree of pavement damage. The study reaches the following conclusions: (1) the strain reversal is induced as the wheels pass through the pavement, and the stress is always a positive value. (2) Both the strain and the stress increase as the loading increases regardless of the loading modes. (3) Comparing the two loading modes at the same velocity and loading, the horizontal tensile strain peak, the horizontal compressive strain peak, and the stress peak are all greater in the single-axle loading mode. But the degree of pavement damage is greater in the dual-axle loading mode based on the points of the time accumulations of strain and stress of each pass.

1. Introduction

The current expressways in China are generally designed for a 15-year service life [1]. However, with the expressway traffic volume, vehicle loading, and tire pressure growing so rapidly, the pavements often deteriorate more quickly than expected [2–4], resulting in a huge economic loss and negative social influence. In order to improve the quality of pavements, the pavement mechanical response to loads, velocity, and tire pressure should be studied. There are now three methods to obtain the pavement mechanical response. The first method is experimenting in the field, the second method is simulating through theoretical calculations, and the third method is measuring through a full-scale accelerated pavement testing (APT) facility. The first two methods have some disadvantages, such as high cost and low precision [5, 6]. APT is a useful tool for evaluating long-term pavement performance in the laboratory [7]. APT is defined as the controlled application of axle loading to pavement structures for the purpose of simulating the effects of long-term in-service loading conditions in a compressed time period [8, 9]. The pavement mechanical response, the design of mixture proportion, and the pavement performances can all be measured using the APT facility. Many valuable results have been discovered using APT, such as follows: (1) there is almost no influence of plate thickness on the vertical compressive stress at the top of the subgrade from the data of the APT test carried out in Austria using the MLS10 facility [10]. (2) The dynamic responses at the bottom of the surface layer captured by the APT facility show that the longitudinal flexural tensile strain presents alternating strain under moving axle loading, and the position only influences its magnitude [11]. (3) When the test is conducted on a semirigid base asphalt pavement on a highway in Chongming Island, Shanghai, China, a fatigue equation of the asphalt layer is established between the loading applications, the strain and the seismic modulus, and a small-strain value of Young's modulus

using the MLS66 facility [12]. (4) The strain at the bottom of flexible base decreases with the increase of velocity but increases with the increase of axle load [13]. Nowadays, the trucks on the expressways are often dual-axle trucks or triaxle trucks, while the existing APT facilities (MLS66, ALF, and HVS) only have a single-axle loading mode. Therefore, the results of the experiments on a regular APT facility cannot reflect the real responses of the pavements on the expressways. The full-scale APT facility developed by Shandong Jiaotong University has two loading modes: the single-axle loading mode and the dual-axle loading mode. Changing between the two loading modes is convenient; thus, a test can work in either of the loading mode at the same velocity, the same equivalent loading, the same tire pressure, the same temperature, and the same pavement structure. This paper describes the structure of the test lane, the sensor processing, and the pavement response to single-axle and dual-axle loading modes. In addition, two parameters are defined to reflect the degree of the pavement damage. This paper also establishes a relationship of the time accumulation of the stress and strain of each pass in between the single-axle loading mode and the dual-axle loading mode.

2. Test Lane

The test lane is located at Shandong Jiaotong University in Jinan, Shandong Province. A pit within the full-scale accelerated pavement loading testing facility allows the prototype-scale pavement sections to be constructed. The APT facility spans the pit and incorporates the capability to apply a moving axle loading to the pavement. The test pit in which the pavement test sections are built is 50 m × 4 m × 2.4 m. The general lane layout is shown in Figure 1. As can be seen, two test lanes are constructed. Both lanes are designed and constructed to have four different sections of different materials and thicknesses within a given test lane. Therefore, the APT facility allows the carriage to pass through four different sections of the lane with simultaneous loadings. In this experiment, the left lane (sections 1, 2, 3, and 4) is used. The right lane (sections 5, 6, 7, and 8) will be used for another rutting and crack experiment.

Pavement structures are designed using Chinese Specifications for Design of Highway Asphalt Pavement [14]. The depth of each structure is 244 cm. The materials for structure 1 and structure 4 are made of AC-13C asphalt mixture, granular base, subgrade (clay), and the original substratum while structure 2 and structure 3 of AC-13C asphalt mixture, granular base, subgrade (silt), and original substratum. In the four structures, eleven strain sensors and four pressure cells are embedded at different depths and positions, which are shown in Figure 2. Nine asphalt strain sensors are placed in the X direction at the bottom of the asphalt mixture and two in the Y direction. Four pressure cells are placed at the top of the subgrade. The thickness of each part is shown in Table 1. The volumetric parameters of the asphalt mixture are shown in Table 2 [15].

2.1. Subgrade. The lower subgrades for all four structures (1 to 4) are processed to a depth of 126 cm from the pavement surface. The clay used in the test lane is from Changqing City, and the silt is from the Yellow River. The materials are compacted into layers using vibratory pad-foot rollers. When the subgrade soil is compacted in the lab using the Proctor compaction test, the resulting maximum dry density of clay is 1.70 g/cm^3 with a corresponding moisture content of 11.40% and the resulting maximum dry density of silt is 2.02 g/cm^3 with a corresponding moisture content of 10.20%. The resilient modulus of the subgrades is tested in different moisture contents according to the T0135-1993 protocol. The test results are presented in Figure 3.

After the construction of the subgrade is finished, ten positions are chosen randomly to measure the penetrations using dynamic cone penetrometers. The results are shown in Figures 4 and 5. The penetration of the silt subgrade from a depth of 30 cm to 50 cm indicates that the compaction in this range is worse than other ranges. The penetration of the clay subgrade is large because the origin soil is still clay below the subgrade, which makes them solid.

2.2. Granular Base. The optimum moisture content and the maximum dry density of the graded broken stone are determined by a field compaction test. The compacted samples should be soaked in water for 96 hours prior to conducting the California Bearing Ratio (CBR) test [16]. The results of the mean value of CBR are no less than 160%.

CBR can be calculated as follows [17]:

$$\mathrm{CBR} = \frac{p}{P_0} \times 100\%, \tag{1}$$

where p is the applied stress in a certain penetration of the tested material and P_0 is the standard stress in the same penetration. According to the JTJ 059-95 [18], penetration = 2.5 mm and P_0 = 7.0 MPa. So the experiment results of three groups are shown in Table 3.

According to the experiment, the optimum moisture content is 2.223 g/cm^3 and the maximum dry density is 5.68%.

2.3. Asphalt Mixture. AC-13C asphalt mixture used in this study is from Zhangqiu City, Shandong Province. The references of the asphalt mixture meet the requirements of JTG F40-2004 [19]. After the paving is completed, seven specimens are taken from the asphalt mixture for the Marshall test. The density, the air void in field, and the compaction degree can be obtained from the test, which is shown in Table 4.

Through extracting and analyzing the asphalt mixture, the asphalt content is 4.87%. Gradation curves for the asphalt mixture using the method of the sieve are shown in Figure 6. From Figure 6, the match of the gradation between the produce and the extraction in the field is good, which means no segregation occurs during the process of transmitting and paving.

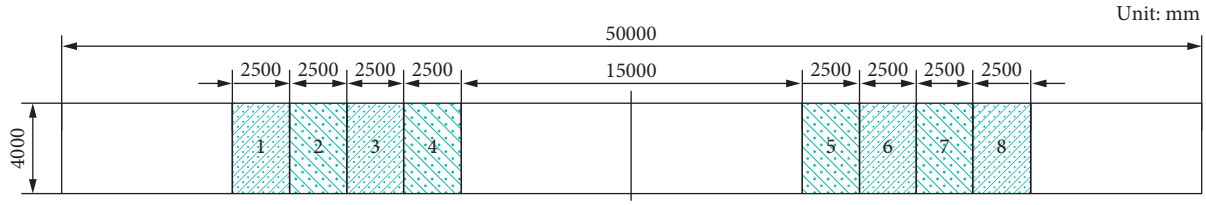

Figure 1: Lane layout.

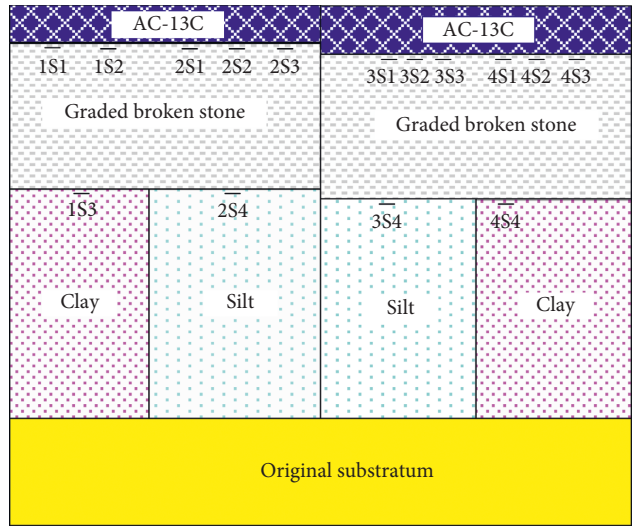

Figure 2: Structure of test lane.

Table 1: Pavement structures.

	Structure 1	Structure 2	Structure 3	Structure 4
Asphalt mixture	7 cm AC-13C	7 cm AC-13C	9 cm AC-13C	9 cm AC-13C
Granular base	39 cm graded broken stone	39 cm graded broken stone	39 cm graded broken stone	39 cm graded broken stone
Subgrade	80 cm clay	80 cm silt	78 cm silt	78 cm clay
Original substratum	118 cm			

Table 2: Volumetric parameters of the asphalt mixture.

Asphalt mixture	Marshall density (g/cm^3)	Bulk density (g/cm^3)	Air void in field (%)	Compactness (%)	Voids in mineral aggregate, VMA (%)	Voids filled with asphalt, VFA (%)
AC-13C	2.46	2.40	6.5	97.6	14.5	65.8

3. Embedded Pavement Sensors

Mechanical responses under the pavement surface are measured with strain sensors and pressure cells. Both device types are considered suitable for measuring dynamic responses only because they experience drift over time that precludes their use in monitoring permanent changes [20]. In the four sections, six stain sensors and one pressure cell are embedded at different depths and positions, which are shown in Figure 7. The asphalt strain sensors are manufactured by Construction Technologies Laboratories (CTL Group) Model ASG-152. A picture of one such sensor placed at the bottom of the asphalt layer, with corresponding dimensions, is shown in Figure 8. The type of the pressure cell is Geokon-3500 manufactured by Geokon. The sensor is constructed from two slightly convex stainless steel plates welded together around its periphery and separated by a narrow gap filled with deaired hydraulic fluid, which is shown in Figure 9. The pressure cell is designated to capture vertical stresses at the top of the subgrade.

4. Pavement Mechanical Response

Accelerated loading is applied with the full-scale APT facility, which is shown in Figure 10. This facility can apply loadings to the pavement in the single-axle or dual-axle loading mode (Figure 11), while all the other existing

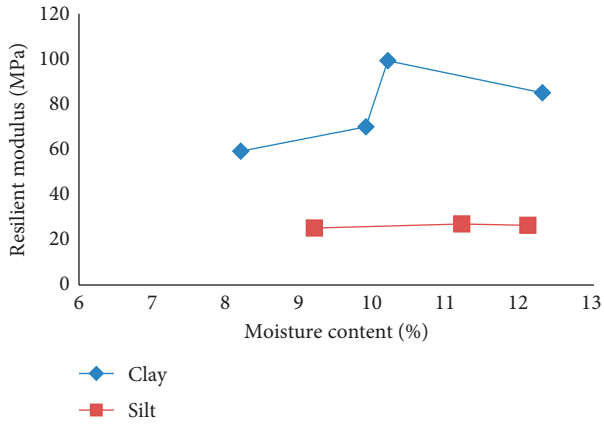

Figure 3: Resilient modulus of subgrade in different moisture contents.

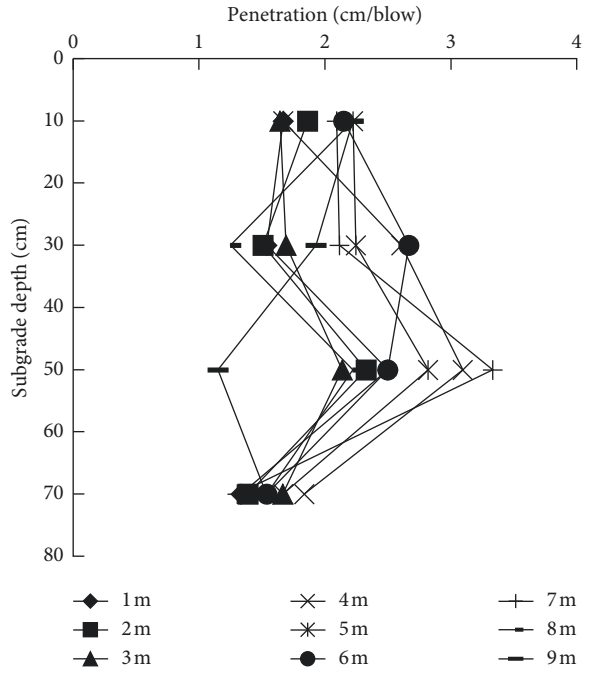

Figure 4: Relationship between penetration and silt subgrade depth.

facilities work only in the single-axle mode. Its main technical parameters are shown in Table 5.

The experiment is finished in different tire pressures, loadings, and velocities, which is shown in Table 6. During the experiment, the temperature of the asphalt layer is held at 28°C ± 2°C. The data of strain and stress are collected by the DATAQ system. The sample frequency of DATAQ is 2 kHz.

4.1. Mechanical Response Affected by Axle Loading in Single-Axle and Dual-Axle Loading Modes. In this paper, one case is selected to analyze the mechanical response. It is assumed that the velocity is 17.7 km/h, the tire pressure is 800 kPa, and the temperature is 26.3°C. The axle loading is variable. The axle loading applied to the pavement is supplied by the

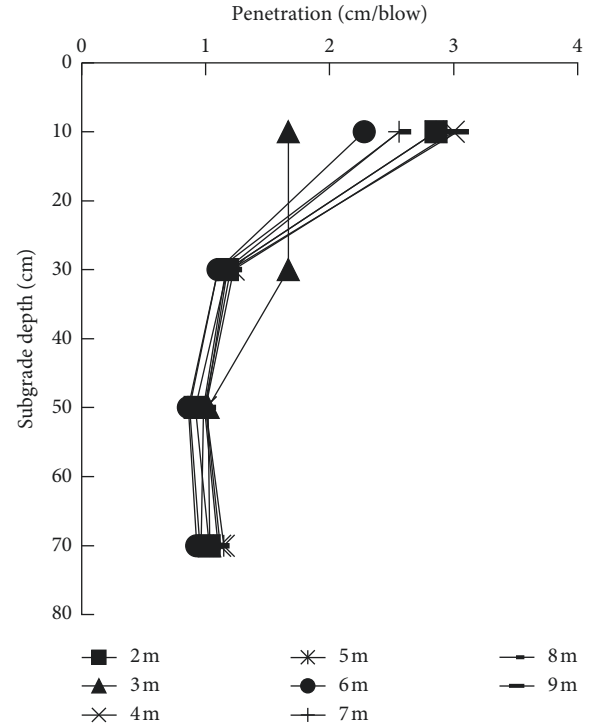

Figure 5: Relationship between penetration and clay subgrade depth.

Table 3: CBR results.

No.	1	2	3
Compaction times	98	98	98
CBR value (%)	202.5	208.7	199.2
Mean value	203.5	203.5	203.5

hydraulic system and calibrated by a dynamic weight gauge. The results of the pavement are shown in Figure 12 at different passes.

The strain and the stress in different loading modes varying with the axle loading in the X direction in structure 3 are shown in Figures 13–16. The maximum and minimum values of the strain are shown in Tables 7 and 8.

The above figures and tables present strains and stresses measured by sensor 3s1 at the bottom of the asphalt mixture in the direction loading. It can be seen as follows:

For strain: (1) The strain reversal is induced into the asphalt mixture as the carriage passes through the pavement in both single-axle and dual-axle loading modes. As the loading approaches, the sensor measures the horizontal compressive strain. The horizontal tensile strain is induced as the carriage gets closer to the sensor, while the strain goes back into horizontal compressive strain as the loading recedes. (2) The approaching branch of the strain response is different from the receding branch, resulting in a nonsymmetrical time-history curve. (3) The horizontal compressive strain peaks are usually higher in the approaching branch than those in the receding branch; the spacing along the

Table 4: Density, air void in field, and compaction degree.

Asphalt mixture	Marshall density (g/cm^3)	Bulk density (g/cm^3)	Air void in field (%)	Compaction degree (%)
AC-13C	2.411	2.530	4.8%	104.9

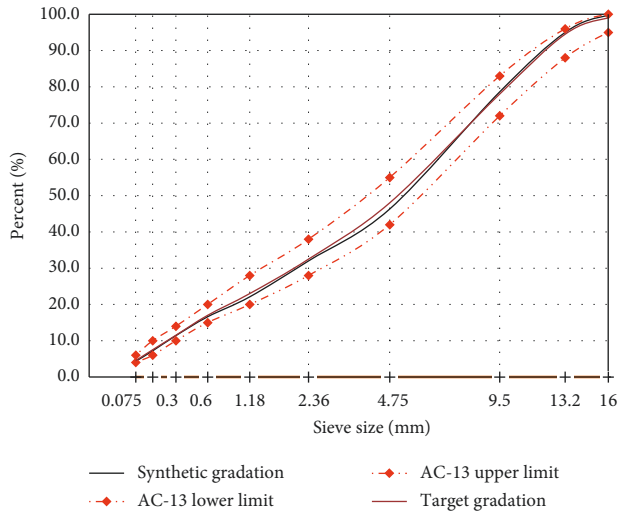

Figure 6: Gradation curves for the asphalt mixture.

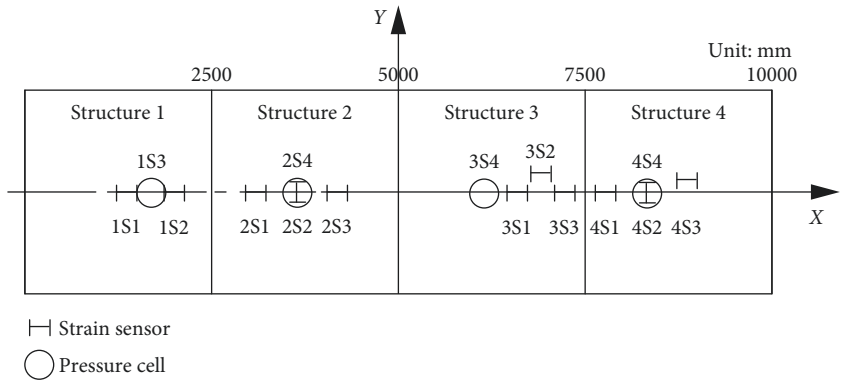

Figure 7: Embedded sensors.

X-axis between the horizontal tensile peaks and horizontal compressive strain peaks is larger in the receding branch than those in the approaching curve. (4) The horizontal tensile peaks and the horizontal compressive strain peaks increase with the increase of the loadings. In the single-axle mode, two horizontal compressive peaks and one horizontal tensile peak occur, while there are three horizontal compressive peaks and two horizontal tensile peaks in the dual-axle loading mode. The first horizontal compressive peak and the horizontal tensile peak present that the front axle is passing. The other peaks present that the rear axle is passing. (5) The horizontal tensile peaks and horizontal compressive peaks in the single-axle mode are higher than the ones in the dual-axle mode. But the loadings are applied to the sensor twice during each pass in the dual-axle mode.

For stress: (1) The stress is always a positive value as the carriage is passing through the pavement. (2) The stress peaks increase with the increase of the loadings. In the single-axle mode, one peak occurs, while there are two peaks in the dual-axle loading mode. The first peak presents that the front axle is passing, and the second peak presents that the rear axle is passing. (3) The peak in the single-axle mode is higher than the one in the dual-axle mode. But the loadings are applied to the pressure cell twice during each pass in the dual-axle mode.

4.2. Time Accumulation of Strain and Stress. In order to study the degree of the pavement damage under long-term cyclic loading, two parameters of the time accumulation of strain and the time accumulation of stress are defined in the paper. The time accumulation of strain is equal to the product of strain and time, and time accumulation of stress is equal to the product of stress and time.

(a)

(b)

Figure 8: Asphalt strain sensor model ASG-152: (a) photograph and dimension of ASG-152; (b) ASG-152 layout.

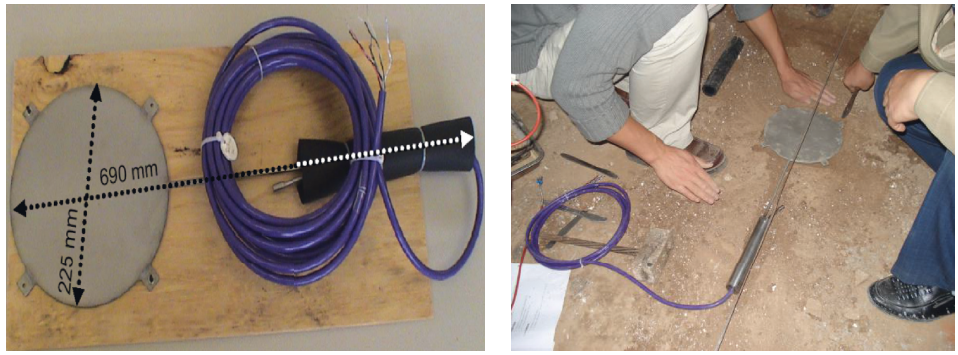

(a) (b)

Figure 9: Pressure cell model Geokon-3500: (a) photograph of Geokon-3500; (b) Geokon-3500 layout.

Assume

$$\begin{aligned} w_1 &= 16.7\text{t}, \\ w_2 &= 13\text{t}, \\ w_3 &= 10\text{t}, \\ v_1 &= 11.4\,\text{km/h}, \\ v_2 &= 17.7\,\text{km/h}, \\ v_3 &= 22.7\,\text{km/h}, \\ v_4 &= 26.5\,\text{km/h}. \end{aligned} \tag{2}$$

During the process of the APT test, the sensors in structure 4 fail, so there no data of the sensor 4S1.

Define

$$\begin{aligned} \Theta &= \zeta t, \\ \Omega &= \xi t, \end{aligned} \tag{3}$$

where ζ is the strain, ξ is the stress, Θ is the time accumulation of the strain each pass, and Ω is the time accumulation of the stress of each pass. Both Θ and Ω can reflect the degree of the pavement damage.

Figure 10: Full-scale APT facility.

(a) (b)

Figure 11: Loading modes: (a) single-axle loading mode; (b) dual-axle loading mode.

Table 5: The main technical parameters.

1	Overall size	Working mode Transporting mode	Length 26342 × width 4220 × height 7934 (mm) Length 26342 × width 3000 × height 3442 (mm)
2	Loading mode	Dual axle Single axle	4 wheels (2 action wheels, 2 driven wheels) 2 wheels (action wheels)
3	Distance between dual axle		1400 mm
4	Maximum loading	Dual axle Single axle	400 kN 200 kN
5	Stable velocity		12~28 km/h
6	Loading length		10 m
7	Rutting depth		80 mm

Table 6: APT loading (S represents single axle, and D represents dual axle).

Tire pressure (MPa)	Axle loading (KN)	Velocity ($km \cdot h^{-1}$)			
0.8	100 (S, D)	11.4 (S)	17.7 (S, D)	22.7 (S, D)	26.5 (S, D)
0.8	130 (S, D)	11.4 (S)	17.7 (S, D)	22.7 (S, D)	26.5 (S, D)
0.8	167 (S)	11.4 (S)	17.7 (S, D)	22.7 (S, D)	26.5 (S, D)
1.0	100 (S)	11.4 (S)	17.7 (S, D)	22.7 (S, D)	26.5 (S, D)
1.0	130 (S)	11.4 (S)	17.7 (S, D)	22.7 (S, D)	26.5 (S, D)
1.0	167 (S)	11.4 (S)	17.7 (S, D)	22.7 (S, D)	26.5 (S, D)

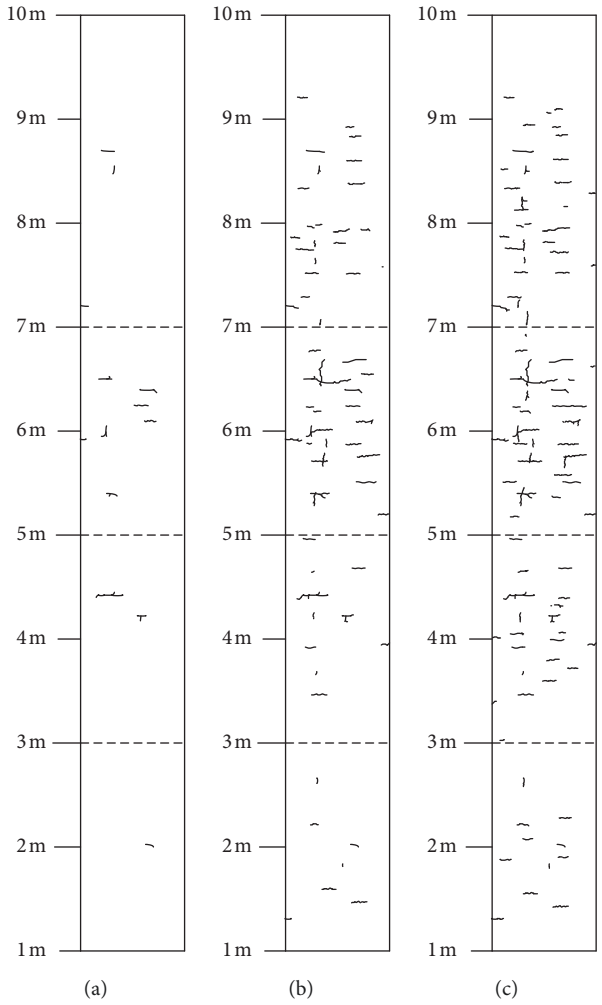

Figure 12: Results of pavement at different passes: (a) 500000 passes; (b) 600000 passes; (c) 700000 passes.

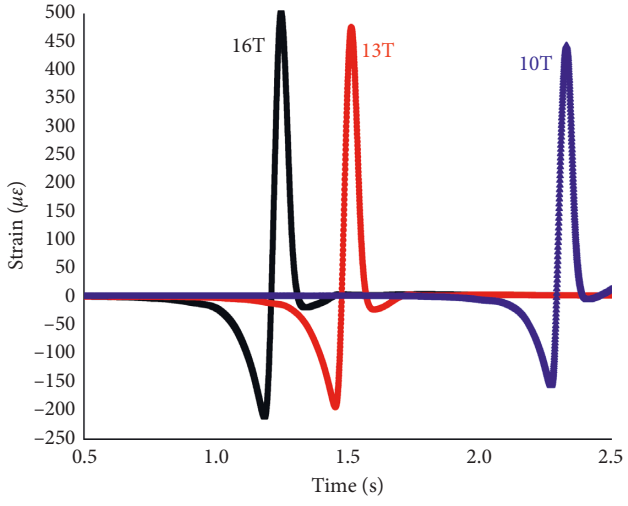

Figure 13: Strain in the single-axle loading mode.

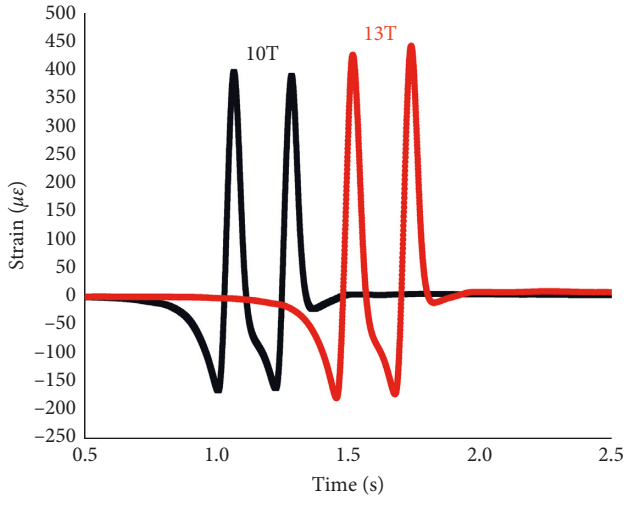

Figure 14: Strain in the dual-axle loading mode.

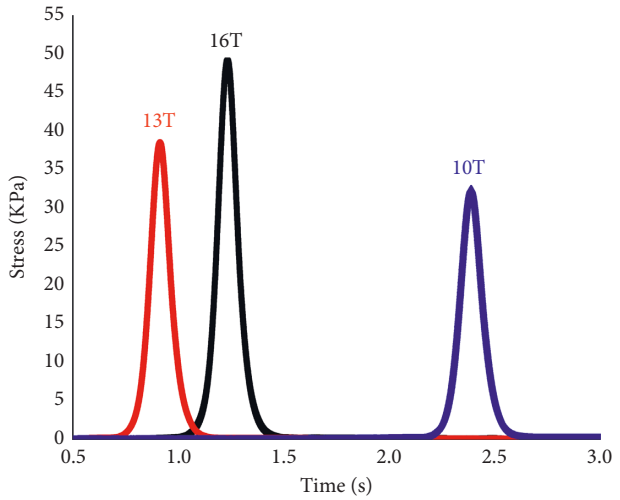

Figure 15: Stress in the single-axle loading mode.

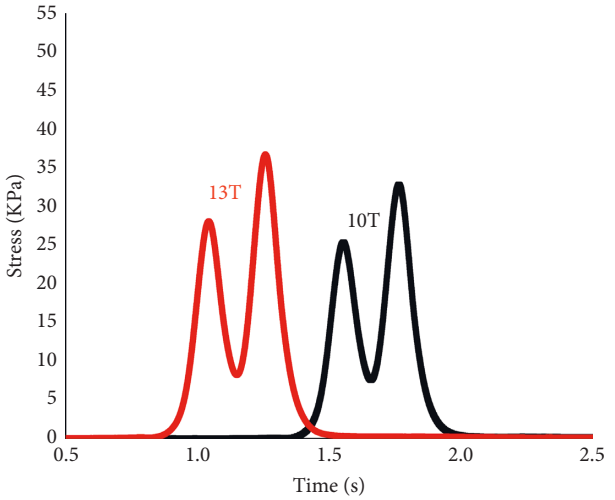

Figure 16: Stress in the dual-axle loading mode.

Table 7: Strain of structure 3 in the single-axle loading mode.

Axle loading (kN)	Maximum horizontal tensile strain, $\mu\varepsilon$	Maximum horizontal compressive strain, $\mu\varepsilon$	Strain value, $\mu\varepsilon$
100	442.9	−157.6	600.5
130	475.6	−195.6	671.2
167	501.3	−212.9	714.2

Table 8: Strain of structure 3 in the dual-axle loading mode.

Axle loading (kN)	Maximum horizontal tensile strain, $\mu\varepsilon$	Maximum horizontal compressive strain, $\mu\varepsilon$	Strain value, $\mu\varepsilon$
100	396.0	−165.6	561.6
130	442.1	−179.1	621.2

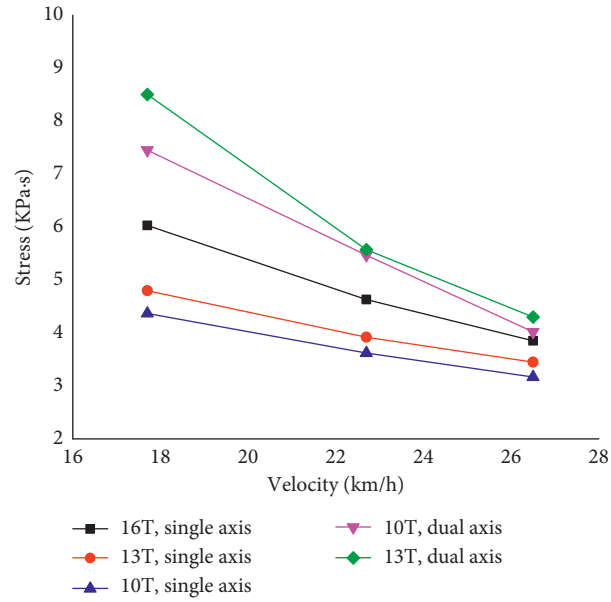

Figure 17: Time accumulation of stress.

Then, the time accumulation of the strains and the stresses of each pass can be obtained as the following equation:

$$\begin{pmatrix} \Theta_{1s1} \\ \Theta_{2s1} \\ \Theta_{3s1} \\ \Theta_{3s2} \\ \Theta_{3s3} \\ \Omega_{2s2} \end{pmatrix} = \begin{pmatrix} \zeta_{1s1} & 0 & 0 & 0 & 0 & 0 \\ 0 & \zeta_{2s1} & 0 & 0 & 0 & 0 \\ 0 & 0 & \zeta_{3s1} & 0 & 0 & 0 \\ 0 & 0 & 0 & \zeta_{3s2} & 0 & 0 \\ 0 & 0 & 0 & 0 & \zeta_{3s3} & 0 \\ 0 & 0 & 0 & 0 & 0 & \xi_{2s2} \end{pmatrix} \begin{pmatrix} t_{1s1} \\ t_{2s1} \\ t_{3s1} \\ t_{3s2} \\ t_{3s3} \\ t_{2s2} \end{pmatrix}$$

$$= \begin{pmatrix} \zeta_{1s1} & 0 & 0 & 0 & 0 & 0 \\ 0 & \zeta_{2s1} & 0 & 0 & 0 & 0 \\ 0 & 0 & \zeta_{3s1} & 0 & 0 & 0 \\ 0 & 0 & 0 & \zeta_{3s2} & 0 & 0 \\ 0 & 0 & 0 & 0 & \zeta_{3s3} & 0 \\ 0 & 0 & 0 & 0 & 0 & \xi_{2s2} \end{pmatrix} \begin{pmatrix} \sum \Delta t_{1s1} \\ \sum \Delta t_{2s1} \\ \sum \Delta t_{3s1} \\ \sum \Delta t_{3s2} \\ \sum \Delta t_{3s3} \\ \sum \Delta t_{2s2} \end{pmatrix}. \quad (4)$$

The time accumulation of the strain and stress value of each pass is easy to calculate through equation (4). The relationship can also be found through the above values between the single-axle and the dual-axle loading modes, which is shown in Figures 17 and 18 and Tables 9 and 10.

From Figures 17 and 18 and Tables 9 and 10, the following conclusions can be obtained:

(1) The time accumulation of strain and stress of each pass in the dual-axle loading mode is higher than that in the single-axle at the same velocity and loading. (2) The time accumulation of strain and stress decreases with the increase of the velocity at the same loading, but the trend is smaller.

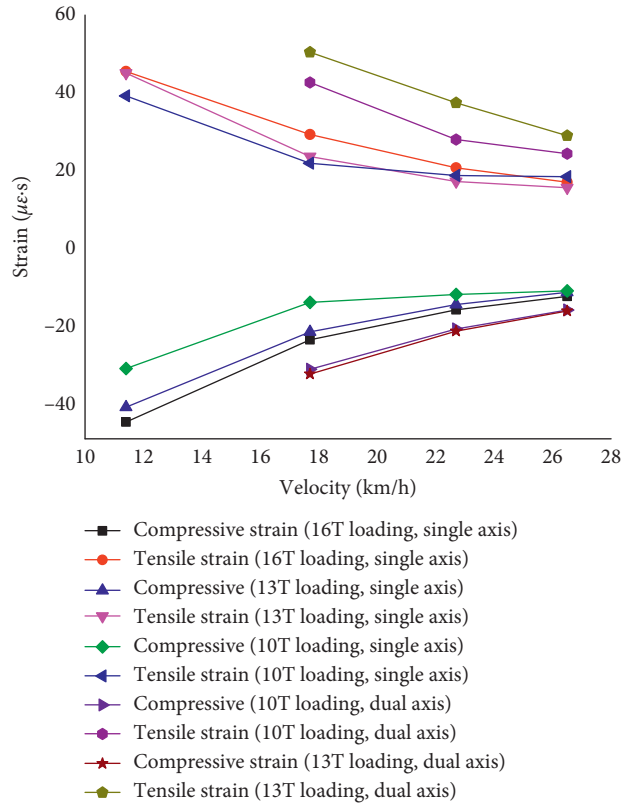

Figure 18: Time accumulation of strain.

Table 9: Time accumulation of strain.

V (km/h)	W (T)									
	16T (single axle)		13T (single axle)		10T (single axle)		13T (dual axle)		10T (dual axle)	
11.4	−45.64	45.34	−41.79	44.92	−31.76	39.02	—	—	—	—
17.7	−24.3	29	−22.24	23.3	−14.6	21.52	−31.96	42.51	−33.19	50.32
12.7	−16.52	20.36	−15.14	16.81	−12.52	18.36	−21.49	27.69	−22.02	37.195
26.5	−13.04	16.59	−11.95	15.15	−11.58	18.03	−16.58	24.01	−16.81	28.71

Table 10: Time accumulation of stress.

V (km/h)	W (T)				
	16T (single axle)	13T (single axle)	10T (single axle)	13T (dual axle)	10T (dual axle)
11.4	9.87	7.72	—	—	—
17.7	6.03	4.8	4.37	7.45	8.5
12.7	4.63	3.92	4.12	5.47	5.57
26.5	3.85	3.45	3.87	4.02	4.3

(3) The time accumulation of strain and stress increases as the increase of the loadings.

5. Conclusions

In the paper, the pavement response in single-axle and dual-axle loading modes is studied using an APT facility that is built with independent intellectual property right. Six strain sensors and one pressure cell are embedded at different depths and positions of the four test structures. The main results can be concluded as follows:

(1) The strain reversal is induced as the wheels are passing through the pavement, and the stress is always a positive value. As the carriage is approaching, horizontal compressive strain is produced and then horizontal tensile strain is induced. But as the carriage is receding, the strain goes back into horizontal compressive strain.

(2) Both the strain and the stress increase with the increase of the loadings. In the single-axle loading mode, there are two horizontal compressive strain peaks: one horizontal tensile strain peak and one stress peak, while there are three horizontal compressive peaks, two horizontal tensile peaks, and two stress peaks in the dual-axle loading mode.

(3) The horizontal tensile strain peak, horizontal compressive strain peak, and the stress peak in the single-axle loading mode are higher than those in the dual-axle loading mode. But the time accumulation of strain and stress of each pass in the single-axle loading mode is smaller than those in the dual-axle loading mode at the same velocity and loading.

(4) At the same conditions, the damage to the pavement in the dual-axle loading mode was greater than that in the single-axle loading mode.

Data Availability

The data used to support the findings of this study are available from the corresponding author upon request.

Conflicts of Interest

The authors declare that there are no conflicts of interest regarding the publication of this paper.

Acknowledgments

This work was financially supported by the Provincial Key R&D Program of Shandong (2016GGX105009) and Shandong Jiaotong University "Climbing" Research Innovation Team Program.

References

[1] J. Wei, L. Wang, and S. Ma, "Modeling mechanical response of a perpetual pavement test road," *Journal of Performance of Constructed Facilities*, vol. 26, no. 2, pp. 153–161, 2012.

[2] Y. Tian, A. Hekmatfar, and J. Haddock, "Comparison of rutting performance between the PURWheel and the NCAT test track," in *Proceedings of the 12th ISAP International Conference on Asphalt Pavements*, Raleigh, NC, USA, June 2014.

[3] Z. Guan, C. Zhuang, and M. Lin, "Accelerated loading dynamic response of full-scale asphalt concrete pavement," *Journal of Traffic and Transportation Engineering*, vol. 12, no. 2, pp. 24–31, 2012.

[4] Q. Liu and D. Cao, "Research on material composition and performance of porous asphalt pavement," *Journal of Materials in Civil Engineering*, vol. 21, no. 4, pp. 135–140, 2009.

[5] J. Chen, J. Liu, Y. Liu, and C. Zhou, "Dynamic responses of asphalt structures under accelerated loading," *Journal of Harbin Engineering University*, vol. 35, no. 6, pp. 771–776, 2014.

[6] I. Al-Qad, S. Dessouky, J. Kwon, and E. Tutumluer, "Geogrid-reinforced low-volume flexible pavements: pavement response and geogrid optimal location," *Journal of Transportation Engineering*, vol. 138, no. 9, pp. 1083–1090, 2012.

[7] M. Arraigada, A. Pugliessi, M. N. Partl, and F. Martinez, "Effect of full-size and down-scaled accelerated traffic loading on pavement behavior," *Materials and Structures*, vol. 47, no. 8, pp. 1409–1424, 2014.

[8] S. Yang, C. Huang, Y. Sun, and H. Susanto, "The development of the scaled accelerated loading simulator facility and transfer functions to the full-scale pavement using theory of similitude by finite element analysis," *International Journal of Pavement Research and Technology*, 2018, In press.

[9] M. Mejías-Santiago, J. D. Doyle, and J. F. Rushing, "Accelerated pavement testing of warm-mix asphalt for heavy-traffic airfields," *Transportation Research Record: Journal of the Transportation Research Board*, vol. 2456, no. 1, pp. 11–20, 2014.

[10] J. Füssl, W. Kluger-Eigl, and R. Blab, "Mechanical performance of pavement structures with paving slabs—part I: full-scale accelerated tests as validation for a numerical simulation tool," *Engineering Structures*, vol. 98, pp. 212–220, 2015.

[11] Z. Dong, Q. Xu, and P. Lv, "Dynamic response of semi-rigid base asphalt pavement based on accelerated pavement test," *China Journal of Highway and Transport*, vol. 24, no. 2, pp. 1–6, 2011.

[12] J. Wu, F. Ye, F. Hugo, and Y. Wu, "Strain response of a semi-rigid base asphalt pavement based on heavy-load full-scale accelerated pavement testing with fiber Bragg grating sensors," *Road Materials and Pavement Design*, vol. 16, no. 2, pp. 316–333, 2015.

[13] W. Wu, L. Zhu, J. Wei, and X. Yan, "Dynamic response analysis of asphalt pavement based on vehicle loading test," *Science Technology and Engineering*, vol. 18, no. 9, pp. 130–135, 2018.

[14] JTG D50-2017, *Chinese Specifications for Design of Highway Asphalt Pavement*, China Communications Press, Beijing, China, 2017.

[15] C. Zhuang, *Structural Design Indexes and Parameters for Flexible Base Asphalt Pavement Based on Accelerated Pavement Testing*, Chang'an University, Xi'an, China, 2012.

[16] R. Taha, O. Sirin, and H. Sadek, "Evaluation of combined excavation waste and reclaimed asphalt pavement aggregates for use in road bases and sub-bases," *Journal of Civil & Environmental Engineering*, vol. 4, no. 2, pp. 1–5, 2014.

[17] S. Bhatt and P. Jain, "Prediction of California bearing ratio of soils using artificial neural network," *American International Journal of Research in Science, Technology, Engineering & Mathematics*, vol. 8, no. 2, pp. 156–161, 2014.

[18] JTJ 059-95, *Field Test Methods of Subgrade and Pavement for Highway Engineering*, China Communications Press, Beijing, China, 1995.

[19] JTG F40-2004, *Technical Specifications for Construction of Highway Asphalt Pavements*, People's Republic of China Industry Standards, Beijing, China, 2004.

[20] E. Levenberg, R. McDaniel, and J. Olek, "Validation of NCAT structural test track experiment using INDOT APT facility," Tech. Rep. 1169, Purdue University, West Lafayette, IN, USA, 2009.